A Novel Fluorescent Sensor Protein for Visualization of Redox States in the Cytoplasm and in Peroxisomes

Taisuke Yano,[1] Masahide Oku,[1] Natsuko Akeyama,[1] Akinori Itoyama,[3] Hiroya Yurimoto,[1] Shusuke Kuge,[2] Yukio Fujiki,[3,4] and Yasuyoshi Sakai[1, 4*]**

Division of Applied Life Sciences, Graduate School of Agriculture, Kyoto University, Kitashirakawa-Oiwake, Sakyo-ku, Kyoto 606-8502, Japan[1]; Laboratory of Microbiology, Graduate School of Pharmaceutical Sciences, Tohoku University, Aza-Aoba, Aramaki, Aoba-ku, Sendai, Miyagi 980-8578, Japan,[2]; Department of Biology, Faculty of Sciences, Kyushu University, Graduate School, Hakozaki, Higashi-ku, Fukuoka 812-8581, Japan[3]; and CREST, Japan Science and Technology Agency, 5, Sanbancho, Chiyoda-ku, Tokyo 102-0075, Japan [4]

Running title: Redox state and peroxisome-deficiency

***Corresponding author.**

Yasuyoshi Sakai, Ph. D.

Division of Applied Life Sciences, Graduate School of Agriculture, Kyoto University, Kitashirakawa-Oiwake, Sakyo-ku, Kyoto 606-8502, Japan.

Tel: +81-75-753-6385. Fax: +81-75-753-6454.

E-mail: ysakai@kais.kyoto-u.ac.jp

****Present address:** Tohoku Pharmaceutical University, 4-4-1, Komatsushima, Aoba-ku, Sendai, Miyagi 981-8558, Japan

Abstract

Reactive oxygen species are generated within peroxisomes during peroxisomal metabolism. However, due to technological difficulties, the intraperoxisomal redox state remain elusive and the effect of peroxisome-deficiency on the intracellular redox state is controversial. A newly developed, genetically-encoded fluorescence resonance energy transfer (FRET) probe, Redoxfluor, senses the physiological redox state via its internal disulfide bonds, resulting in a change in conformation of the protein leading to a FRET response. We made use of Redoxfluor to measure the redox states at the subcellular level in yeast and Chinese hamster ovary (CHO) cells. In wild-type peroxisomes harboring an intact fatty acid β-oxidation system, the redox state within the peroxisomes was more reductive than that in the cytosol, despite the fact that reactive oxygen species were generated within the peroxisomes. Interestingly, we observed that the redox state of the cytosol of cell mutants for peroxisome-assembly, regarded as models for a neurological metabolic disorder, was more reductive than that of the wild-type cells in yeast and CHO cells. Furthermore, Redoxfluor was utilized to develop an efficient system for screening of drugs that moderate the abnormal cytosolic redox state in the mutant CHO cell lines for peroxisome assembly, without affecting the redox state of normal cells.

Introduction

Peroxisomes are single-membrane bound organelles harboring at least one H_2O_2-generating oxidase and one H_2O_2-decomposing catalase, and are present in virtually all eukaryotic cells, from yeast to mammals. The most conserved activity of peroxisomal metabolism is the β-oxidation of fatty acids (26).

Peroxisome assembly requires more than 20 *PEX* gene products, termed peroxins in any given organism (5). The impairment of peroxisomal protein transport caused by mutations in *PEX* genes causes fatal human peroxisome biogenesis disorders (PBDs) (33). In the cells of such PBD patients, essential enzymes normally localized to peroxisomes are mostly found in the cytosol. Mammalian cell lines harboring mutations in peroxins (including fibroblasts from PBD patients) grow well in cell culture. On the other hand, *pex* mutants of the methylotrophic yeast *Pichia pastoris* can grow normally on glucose, but not oleate or methanol (37).

Peroxisomal metabolic pathways can generate a high level of reactive oxygen species (ROS) (31). Therefore, peroxisomal disorders have been studied with a focus on the generation of ROS. However, the relationship between PBDs and the intracellular redox state is unclear (12, 31).

Peroxisomes have long been thought to be in a more highly oxidized state than the cytosol due to this generation of ROS. However, there is no reported experimental evidence supporting this notion. We previously identified a 20-kDa peroxisomal membrane protein, named Pmp20, in methanol-induced peroxisomes of methylotrophic yeasts. Pmp20 had a glutathione peroxidase activity, suggesting the presence of glutathione within the peroxisomes (9). However, we and other groups of investigators have been unable to determine the levels of the reduced and oxidized forms of glutathione due to technical difficulties, and therefore have been unable to

assess the redox state within peroxisomes by conventional biochemical methods.

In general, the intracellular redox state is determined by the levels of redox-related metabolites that are generated by multiple metabolic pathways. (We herein refer to the "redox state" as an intracellular environment at steady state, which is distinct from "oxidative stress" or "ROS" which functions as a signal for further intracellular events such as apoptosis.) Therefore, the redox state is considered to reflect the overall metabolic status. While the standard redox potential (E_0') is a general index used to express the redox state of a compound, it cannot be used to describe the intracellular redox state because it does not take into account various physiological considerations, such as in the cytosol where many compounds co-exist in a mixture of various redox states (13). Therefore, the equilibrium redox state in living cells has been estimated from indices such as the ratio of oxidized and reduced forms of glutathione, or from indirect indices of the redox state, such as the NAD(P)H ratio (11, 40), or the level of expression of antioxidant enzymes. However, measurement of these indices often yields contradictory results, making it difficult to evaluate the physiological redox state using any single index. This situation might have led to misunderstanding the redox state in cells from patients with PBDs. Reductive conditions could occur during conditions of oxidative stress, when the ROS defense system is functioning normally.

With the aim of determining the intracellular redox state directly, we developed a fluorescent redox probe, Redoxfluor, with a novel sensing mechanism. Several green fluorescent protein (GFP) variants that report the *in vivo* redox state [roGFP (4, 7), rxYFP (17, 23, 24)] or H_2O_2 level [HyPer (3)] have been developed since the start of our research. However, none of these reporters have been used to visualize the redox state in mammalian cytosol, and differences in the redox potential

between normal and pathological states have not been reported.

In the present work, we developed Redoxfluor that discriminates the redox state of peroxisome assembly mutant cell lines (33) from that of the normal cell line. Our findings shed light on how to tackle problems with monitoring the spatiotemporal dynamics of the redox state within living mammalian cells and should also pave the way for the development of a screen for drugs that can affect various metabolic disorders with abnormal redox state.

MATERIALS AND METHODS

Construction of plasmids driving expression of Redoxfluor. A recombinant gene encoding Redoxfluor (Fig. 1A) was constructed as follows: the DNA fragment encoding Yap1 CRD (I601 to N650) DNA was amplified by PCR using either one of the two primer sets: 1) a forward primer containing an *Sph*I site and a reverse primer containing sequences encoding a short linker (GG) and a *Cla* I site, or 2) a forward primer containing *Cla* I site and a reverse primer containing *Sac* I restriction site. The two PCR products were ligated, fused at the 5' end to a DNA fragment encoding Cerulean (28) (a version of enhanced cyan fluorescent protein, or CFP) and at the 3' end to a DNA encoding Citrine (6) (a version of enhanced yellow fluorescent protein, YFP) (Fig. 1A). The constructed Redoxfluor C-probe DNA was cloned into the $pRSET_A$-vector with N-terminal hexa-His tag (His_6) (Invitrogen) for expression. The plasmid encoding Redoxfluor A-probe was generated from the plasmid encoding Redoxfluor C-probe using QuikChange PCR-based mutagenesis kit (Stratagene).

Expression and Purification of Redoxfluor. *E. coli* BL21 (DE3) cells were transformed with the constructed expression plasmids encoding Redoxfluor A- or C-probe. Cultures of the transformants grown in L-broth at log phase (OD_{610} = 0.5) were treated with 0.5 mM isopropyl-β -$_D$-thiogalactopyranoside (IPTG) for 12 h at 23°C to induce expression of Redoxfluor. Cells were collected and lysed by sonication in buffer A (300 mM NaCl, 50 mM NaH_2PO_4, 10 mM imidazole, pH 8.0). His-tagged Redoxfluor was purified by two cycles of chromatography on a column of Ni-nitrilotriacetic acid (Ni-NTA) agarose (Qiagen) according to the manufacturer's instructions. Proteins were quantified by Bradford's method with the use of a Protein Assay kit (Bio-Rad) with bovine serum albumin (BSA) used as the standard.

Redox titration of Redoxfluor *in vitro.* The redox potentials of Redoxfluor were determined from its reaction with glutathione. Purified Redoxfluor (0.3 μM) was incubated in RT buffer (75 mM HEPES-KOH (pH 7.0), 140 mM NaCl, 1 mM EDTA) containing concentrations of GSH and GSSG varying by 1 mM increments. After equilibration of the protein samples for 20 h at 37°C, the fluorescence emission spectra were collected on a RF5300PC spectrofluorophotometer (Shimadzu Co. Ltd.) at 405 nm or 434 nm excitation. All manipulations were carried out in an anaerobic chamber (Coy Laboratory products).

Biochemical analysis of Redoxfluor with mPEG-maleimide. For *in vitro* analysis, purified Redoxfluor proteins equilibrated with GSH/GSSG as described above were incubated with 10 mM (final concentration) of mPEG-maleimide (Laysan Bio) at 30°C for 30 min. The sample was mixed with 1/3 volume of SDS sample buffer [50 mM Tris-HCl, pH 6.8, 30%(v/v) glycerol, 3%(w/v) sodium dodecylsulfate, 6% (v/v) 2-mercaptoethanol, and 60 mg/L bromophenol blue], and boiled for 1 min. For *in vivo* assessments of redox states, CHO cells were cultured on 90 mm-diameter culture dishes to semi-confluency, washed twice with ice-cold phosphate-buffered saline (PBS), and lysed in 100 μl of ice-cold PBS containing 0.5% (v/v) of Tween 20 and Complete proteinase inhibitor cocktail (Roche). The protein concentration of the lysate was adjusted to 1 mg/ml in the same buffer used for cell lysis, and the samples (each 180 μl) were incubated with mPEG-maleimide and then SDS sample buffer as described above. The samples were subjected to SDS-PAGE with 0.5% (v/v) 2-mercaptoethanol contained in the running buffer, transferred to Immobilon-P PVDF membrane (Millipore), and analyzed by immunoblot analysis using a 3,000-fold dilution of rabbit anti-GFP antiserum (Invitrogen).

Plasmids for expression of Redoxfluor, cells and growth conditions. The *S. cerevisiae* strain used in this study was BY4741 (*MATa his3Δ1 leu2Δ0 met15Δ0 ura3Δ0*) (22). For expression in *S. cerevisiae*, Redoxfluor was subcloned into the pRS416 *CEN* vector containing the *GAP* promoter and terminator. For expression in *P. pastoris* strain PPY12 (*arg4 his4*) (30), Redoxfluor was subcloned into the integrating pIB2 vector (32) containing the *GAP* promoter. The isogenic *Pppex5*Δ and *Ppcta1*Δ strains were generated by replacing the respective coding region with *Zeo*^{r} gene. For mammalian expression, we chemically synthesized the Yap1 CRD region of Redoxfluor with the preferred codon usage and cloned the sequence into pIRESpuro3 (Clontech) downstream of a Kozak consensus sequence (15) (GCCGCCACC-ATG). For C-probe-PTS1, the C-probe was extended by PCR at the 3' end with a sequence encoding the peroxisomal targeting signal (PTS1) (21). CHO cells were transfected with plasmid constructs using Lipofectamine^{TM} 2000 (Invitrogen).

For the oxidative stress assay, *S. cerevisiae* and *P. pastoris* were grown at 28°C in SD medium (0.67% yeast nitrogen base and 2% glucose) supplemented with amino acids and transferred to the same medium containing either of H_2O_2 (100 μM), ATZ (10 mM) or BSO (100 μM). For microscopic analyses of *P. pastoris* strains under peroxisome-inducing conditions, the cells were grown at 28°C for 16 hours in SM medium (0.67% yeast nitrogen base without amino acids and 0.5% methanol) or YNO medium (0.67% yeast nitrogen base, 0.05% yeast extracts, and 0.5% oleate) supplemented with their auxotrophic amino acids (100 μg/mL). CHO cell lines were grown in Ham's F-12 medium supplemented with 10% (v/v) FCS under 5% CO_2/95% air.

Fluorescence microscopy. We performed light microscopic imaging using a fluorescence-inverted microscope (IX70; Olympus) equipped with an Uplan Apo 100x/1.35 oil iris for yeast cells or LUCPlanFLN 40x/0.60 Ph2 dry iris objective lens for CHO cells using mirror/filter units XF88-2 (Omega Optical, Inc.) for CFP/YFP FRET and U-MNIBA (Olympus) filter set for GFP. Images were captured with a charged-coupled device camera (Sensys; PhotoMetrics) and analyzed using the MetaMorph software package version 7.0 (Universal Imaging Corp). For the evaluation of FRET values of the cytoplasm or peroxisomes, more than 20 regions in each acquired FRET image were selected and subjected to 'Region Measurements' using the above-mentioned software.

qRT-PCR. Total RNA was isolated from cells at log-phase using the RNeasy mini kit (Qiagen) followed by on-column DNase digestion. cDNAs were synthesized from 1 μg total RNA using Random Primers (Promega) and ReverTra Ace (Toyobo). After reverse transcription for 50 min at 42°C, the samples were heated for 5 min at 99°C to terminate the reaction, and 0.5 μl of RNase H was added. qRT-PCR was performed in 20 μl mixtures in glass capillary tubes in a LightCycler (Roche Diagnostic). Primers used for the reactions are listed in Supplementary Table 1. Negative control PCR reactions were performed without ReverTra Ace addition.

Determination of glutathione. CHO cells were grown to confluence in the presence or absence (control culture condition) of pharmacological agents for 24 h. *P. pastoris* cells were cultured to mid-log phase in YNO medium at 30°C. CHO and yeast cells were harvested by centrifugation, washed once with physiological saline, and disrupted with zirconia beads in 300 μl of ice-chilled 8 mM HCl solution. Cell homogenates were centrifuged at 12,000 x g at 4°C, and the amount of GSH and GSSG in the resultant supernatant was determined as previously described (35).

RESULTS

Development and characterization of Redoxfluor as a redox indicator. The yeast transcriptional factor Yap1 senses the intracellular redox state via its carboxy-terminal cysteine-rich domain (c-CRD) (16), and the structure of c-CRD has been reported to reflect the equilibrated and steady-state physiological redox status (1). The Redoxfluor C-probe (C-probe) contains a tandem repeat of the partial sequence for c-CRD (Yap1 601-650) (Fig. 1A), and mediates fluorescence resonance energy transfer (FRET) between Cerulean (28) (CFP) and Citrine (6) (YFP) (Fig. 1B). Exposure of the purified C-probe to H_2O_2 enhanced the CFP emission at the expense of the YFP emission, and decreased the yellow-to-cyan emission ratio (527/476 nm), indicating an H_2O_2-induced loss of FRET (Fig. 1B and C).

Next, the purified C-probe was used for determination of the FRET ratio (the fluorescence intensity of YFP divided by that of CFP) in titration buffers containing various ratios of reduced (GSH) and oxidized (GSSG) glutathione (Fig. 2A). Based on the Nernst equation with an E_0 value of -240 mV for the GSH/GSSG redox couple (29), the redox midpoint potential of the C-probe was determined to be -213 mV at pH 7.0 and 30°C, which was close to the value of the mammalian cytosolic redox potential (10). From the titration curve, the redox potential within the range of ~-180 to -250 mV can be estimated from the FRET ratio (Fig. 2A). Under the conditions used for our experiment *in vitro,* this titration curve was unaffected by the probe concentration within a range up to 1 μM (data not shown), which is estimated to be a much greater concentration than the level of the intracellularly expressed Redoxfluor and much lower than the intracellular GSH + GSSH concentration (0.5-10 mM) (14). Thus, the effect of intracellular expression of Redoxfluor on the redox state was assumed to be negligible.

The redox-dependent FRET response of the C-probe was supported by experiments using the control Redoxfluor A-probe (A-probe), in which all of the redox-sensitive cysteine residues in the C-probe CRD had been replaced by alanine (Fig. 2A). The A-probe did not show the C-probe-like FRET response following exposure to oxidizing reagents, although we observed a slight change in FRET due to the inherent redox-responsive nature of the fluorescent protein. This CRD-independent FRET change was reduced by the use of Cerulean and Citrine instead of the original CFP and YFP, and the former combination of fluorescent proteins gave rise to a larger change in FRET than did the latter combination (data not shown).

The CRD-dependent oxidation of the C-probe was confirmed by biochemical experiments that involved conjugation of methoxy-Poly (Ethylene Glycol)-maleimide (mPEG-maleimide) to free thiol residues within the probe proteins, resulting in incremental increases in size of the probe proteins that could be detected by immunoblot analysis (Fig. 2B). Consistent with the FRET ratio analysis, the fraction of C-probe protein modified with mPEG-maleimide decreased as the redox potential of the GSH/GSSG titration buffer increased. In contrast, similar treatment of A-probe protein did not show any change in the mobility of the protein as assessed by immunoblot analysis (Fig. 2B). The C-probe responded to redox reagents within a pH range of 6.5 to 8.5 (Fig. S1). Unlike the case with other fluorescent redox probes, such as roGFP, we were able to make use of the A-probe as a control that enabled us to assess the true redox-dependent conformational change of the C-probe.

Redoxfluor is an intracellular redox indicator. Redoxfluor was then expressed in the yeast *Saccharomyces cerevisiae* and Chinese hamster ovary (CHO) cells (with optimized codon usage), which were subsequently subjected to conventional FRET

imaging analysis (Fig. 3). We observed a change in the cytosolic FRET image of the C-probe from green (reducing) to blue (oxidizing) in response to treatment of both types of cell with either oxidative agents such as H_2O_2, or non-oxidative reagents, such as 3-amino-1,2,4-aminotriazole (ATZ), an inhibitor of catalase, or buthionine sulfoximine (BSO), an inhibitor of glutathione synthesis (Fig. 3A and B; Video 1 and Video 2). In contrast, neither ATZ nor BSO led to a change in the FRET signal *in vitro* (Fig. 1C), indicating that the observed change in the FRET signal *in vivo* reflects an effect upon cellular metabolism rather than a direct effect of these reagents on the C-probe. Similar results were obtained in cells of the methylotrophic yeast *Pichia pastoris* expressing the C-probe (Fig. S2).

Analysis of cells following removal of H_2O_2 or ATZ from the culture media led to reduction of the redox state of the cytosol (Fig. 3A and B), demonstrating that the C-probe responds to the redox state in a reversible manner in yeast and CHO cells. This reversibility of the C-probe response was seen even in the presence of cycloheximide (Fig. S3), demonstrating that the reversibility of the probe response was real and not merely due to the synthesis of new probe following wash out of the drug.

Redox state within peroxisomes. We next genetically engineered derivatives of the Redoxfluor C- and A-probes harboring C-terminal peroxisome targeting signal 1 (PTS1) (21). The subcellular localization of these probe proteins exhibited a punctate pattern when expressed in wild-type CHO cells (Fig. 4A), but exhibited a disperse pattern of distribution following expression in temperature-sensitive, *pex5* mutant CHO cells ZP105, which verifies the targeting of the probe proteins to the peroxisome.

Using these peroxisome-targeted probes, we found that the intraperoxisomal redox state is more reductive than that of the cytosol in wild-type CHO cells (Fig. 4A).

We observed that both the cytosolic and intraperoxisomal redox states became oxidative following exposure of the cells to either ATZ or H_2O_2 (Fig.4B; Video 3), thereby demonstrating that the C-probe functioned normally in peroxisomes and that the peroxisomes were in a reductive state in CHO cells.

We next introduced the peroxisome-targeted Redoxfluor into the methylotrophic yeast *P. pastoris*. In this yeast, peroxisomes can be induced by culture on either oleate or methanol as a sole carbon source. The oleate-induced peroxisomes contain a fatty acid β-oxidation system similar to that in mammalian peroxisomes, whereas methanol-induced peroxisomes contain enzymes for methanol metabolism that are specific to the methylotrophic yeasts. We performed the FRET ratio analysis in these cells, and observed that the redox state within the oleate-induced peroxisomes was more reductive than that in the methanol-induced peroxisomes (Fig. 4C). These results demonstrate that changes in the intraperoxisomal redox state can be monitored using Redoxfluor and that the redox state within peroxisomes depends on the carbon source used to induce peroxisome proliferation.

Cytosolic redox state within peroxisome-assembly mutant cell lines. We next applied Redoxfluor to investigate the relationship between the cytosolic redox state and peroxisomal disorders. For this purpose, the cytosolic Redoxfluor C-probe was introduced into the temperature-sensitive *pex5* mutant cell line, ZP105. We observed a more reductive cytosolic redox state in the mutant ZP105 cells than in wild-type CHO cells at the non-permissive temperature (37°C) (Fig. 5A and B). And the cytosolic redox state of ZP105 cells became more oxidative following the decrease of the culture temperature to 30°C for 7 days. This change in the redox state of ZP105 cells was accompanied by recovery of the peroxisomal import of GFP-PTS1 (Fig. 5B)

and PTS2 proteins (data not shown). On the other hand, we did not observe differences in the redox state in the wild-type CHO cells between the culture temperatures at 37°C and 30°C (Fig. 5A and B). These experiments demonstrate that the steady-state cytosolic redox equilibrium is more reductive when peroxisome assembly is impaired.

In order to verify the microscopic results showing a more reductive redox state in the *pex* mutant cell line, cell lysates were prepared from the Redoxfluor-expressing cells and subjected to biochemical analysis using mPEG-maleimide (Fig. S4). Incubation of cell lysate with this reagent led to a greater degree of modification of the probe proteins compared to that observed in the corresponding *in vitro* analyses (Fig. 2B), presumably due to a reduced level of thiol-containing substances (which could compete with the probe proteins for modification by mPEG-maleimide) upon cell breakage. Comparison of the intensities of the immunoblot signals indicated that the probe proteins in the lysate prepared from the *pex5* cells were modified to a slightly greater extent by mPEG-maleimide, although the difference was very small.

Next, we compared the microscopic results using Redoxfluor with those obtained using conventional redox indices: the ratio between the oxidized and reduced forms of glutathione and the expression ~~level~~ of antioxidant enzymes (8, 27). In good agreement with the FRET imaging, we observed decreased *GST* transcription at 37°C and 30°C in ZP105 cells, relative to the level observed in the wild-type cells (Fig. 5C). This reductive cytosolic redox state in ZP105 cells at 37°C and its shift at 30°C to a level similar to that observed in the wild-type cells were also confirmed by measurement of the intracellular GSH/GSSG ratio (Fig. 5D). Taken together, these data demonstrate a more reductive state of the cytoplasm in the *pex5* strain, that was readily observed by FRET imaging using Redoxfluor.

The more reductive state in the cytoplasm of peroxisome-assembly mutant cells was also observed in *P. pastoris pex2*Δ and *pex5*Δ cells transferred to oleate medium (Fig. 6A). This may be partly due to lower levels of H_2O_2 generation in the mutant strains. Acyl-CoA oxidase is a major peroxisomal H_2O_2-generating enzyme that is found degraded in the cytosol of *pex* mutants of both mammalian and yeast cells (36). As such, the difference between the redox state observed in normal cells and peroxisome-assembly mutants might reflect differences in the efficiency of generation and elimination of H_2O_2 between the wild-type and mutant cells. This notion is supported by the observation that ROS accumulation is more readily detected in CHO-K1 (wild-type) cells than in ZP105 cells using the fluorescent ROS indicator, 2',7'-dichlorodihydrofluorescein diacetate (DCF) (Fig. S5). The import of catalase was not restored in ZP105 cells following culture at 30°C for 7 days, which is reminiscent of the phenotype of infant Refsum disease, a milder form of PBD (Fig. 5B) (25). These results suggest that mislocalization of peroxisomal catalase is not the main cause of abnormal reductive states observed in cells mutant for peroxisome assembly.

The findings that mitochondrial manganese-superoxide dismutase is strongly expressed in PBD cell lines has led to the conclusion that PBD cell lines suffer from oxidative stress (2). The level of transcription of genes encoding several antioxidant enzymes in *P. pastoris* was compared between the wild-type and *pex5* mutant strains (Fig. 6B). The lower level of expression of *PpGPX* (glutathione peroxidase) and *PpTSA1* (cytosolic thioredoxin peroxidase) in the *Pppex5*Δ cells suggested that the *Pppex5*Δ cells are in a reductive state. Meanwhile, the transcription level of *PpCTA1* (catalase) and *PpSOD2* (mitochondrial manganese-superoxide dismutase) was greater in the same mutant than in the wild-type cells, suggesting a greater level of ROS

generation in the *Pppex5*Δ cells. These results imply that the cytosol could be in a reductive state even under conditions of oxidative stress owing to a greater level of expression of anti-oxidant genes induced following generation of ROS in these cells under these conditions.

Screening for "redox modulators". We finally made use of Redoxfluor in the development of a screen for "redox modulators" that can restore the redox state in the patient-derived cells to a level similar to that observed in wild-type cells without affecting the redox state in normal cells. Several pharmacological agents have been suggested as potential therapeutics to treat milder forms of PBD (12, 13, 18-20, 38). We examined whether such agents could alter the intracellular redox state using Redoxfluor. Exposure of cells to Trichostain A (TSA), a histone deacetylase inhibitor, narrowed the difference between the redox states observed in CHO-K1 (wild type) and ZP105 cells at 37°C (Fig. 7A). TSA was more effective in doing so than either tocopherol (VE) or another histone deacetylase inhibitor, 4-phenylbutyrate (4PBA). In contrast, TSA treatment led to only a small change in the redox state of wild-type CHO-K1 cells (Fig. 7A). VE treatment led to a small change in the redox state to a more oxidative level in ZP105 cells, despite the fact that Kawada et al. speculated that VE can act as an antioxidant in PBD cell lines (12). The effects of the drugs observed by FRET-ratio imaging were verified by analyses of both the level of GST transcription and GSH/GSSG ratio, in that TSA was also observed to narrow the differential between these indices between the wild-type and ZP105 strains more efficiently than the other compounds tested (Fig. 7C and D). The level of ROS accumulation in drug-treated ZP105 cells detected by DCF paralleled the change in redox state visualized by Redoxfluor (Fig. S5), confirming the validity of the microscopic assessment.

DISCUSSION

With the Redoxfluor probe developed in this study, we were able to visualize pathological redox states of a metabolic disorder in cells mutant for peroxisome assembly. Visualization of the redox state at the subcellular level has revealed that to our surprise the intraperoxisomal redox state is maintained in a reductive state in CHO cells, despite the generation of ROS by normal peroxisomal metabolism. This was unexpected because peroxisomes express numerous oxidative metabolism pathways and have been long thought to exist in an oxidized state. The difference between the cytoplasmic redox potential of wild-type and *pex5* CHO cells at 37°C was estimated to be approximately 9 mV (-217 mV in the wild-type versus -226 mV in the *pex5* cell line) when the FRET ratio monitored following excitation at 405 nm using a confocal spectrophotometric imaging system (Zeiss LSM510 META) was compared with the titration curve generated from the *in vitro* data (see Fig. 2A). This small difference detected by using Redoxfluor would be difficult to detect using a biochemical assay (Fig. 5 and Fig. S4). We are confident that the FRET signal generated by using Redoxfluor can be used directly as an index of the equilibrated redox state in a cell, shedding light on the physiological and pathological significance of the change in the steady-state redox potential caused by a metabolic defect.

In cells, the equilibrated redox state is established by the levels of various redox-related metabolites, such as GSH, NAD(P)H, thioredoxin, and ROS. Therefore, the redox state is considered to reflect the overall metabolic status. This study revealed that peroxisomes induced for oleate metabolism were more reductive than those induced for methanol metabolism in *P. pastoris*. This observation seems to reflect the fact that the high-energy bonds of fatty acid thioesters are stabilized in peroxisomes during β-oxidation. On the other hand, during methanol metabolism, the

reduced glutathione within peroxisomes is consumed through two critical reactions for methanol metabolism, i.e., by forming hydroxymethyl glutathione non-enzymatically and by being further oxidized to S-formylglutathione to metabolize formaldehyde (39), or by Pmp20-glutathione peroxidase to detoxify intraperoxisomal ROS (9).

In many genetic disorders such as PBDs, where gene therapy is not a practical approach, drugs are used for symptomatic treatment. Desirably screening of such drugs is performed using cultured cells. The results obtained here using CHO cell *pex* mutants and PBD cell lines strongly suggest that an oxidative redox state is not the direct cause of PBDs. We believe that any metabolic deficiency owing to the dysfunctions of peroxisomes in the PBD cell lines, such as the impaired peroxisomal fatty-acid β-oxidation, readily gives rise to an imbalance in overall cellular metabolism, resulting in a reductive cytosolic state. Therefore, the redox state in CHO cells mutant for peroxisome assembly may reflect the degree of metabolic abnormality that is correlated to the severity of PBDs. In this context, it is plausibe that TSA treatment (Fig. 7) may modulate metabolic defects arising from the peroxisomal abnormalities, whereas in the wild-type cell line these defects are not induced and the cells are thus not affected by the drug application.

A genetically-encoded redox probe, roGFP (7), was recently used to visualize the redox status in plant leaf cytosol (around -310 mV) (34) and also in yeast and mammalian cells that were exposed to oxidoreductive reagents, including H_2O_2 and DTT (4). However, the roGFP probe did not respond to cell treatment with non-oxidative reagents such as ATZ, a catalase inhibitor. Moreover, roGFP showed only a small change in the fluorescence spectrum following exposure of cells to buthionine sulfoximine (BSO), an inhibitor of glutathione synthesis. These results imply that

roGFP is neither sufficiently sensitive to visualize the redox dynamics at the physiological level in the cytosol nor sufficiently sensitive to distinguish the differences in the redox state between normal cells and patient-derived cell lines. Even the spectrum of the original GFP and other fluorescent proteins (not developed as redox probes) are known to be affected by some intracellular environment, e.g., pH, temperature, or redox state. Unlike the case with roGFP, the control Redoxfluor A-probe made it possible to confirm that the change in the conformation of the Redoxfluor C-probe in living cells is CRD-dependent.

We are currently attempting to identify and characterize metabolites that contribute to the reductive state in mutant cells for peroxisome assembly by several approaches, including metabolome analysis. Since Redoxfluor can discriminate between physiological and pathological redox states, it may be possible to screen for compounds that can modulate the intracellular redox state in cells of patients with abnormal redox potential.

ACKNOWLEDGEMENTS

This paper is dedicated to the late Koichi Suzuki, Research Supervisor, CREST, Research Area "Basic Technologies for Controlling Cell Functions Based on Metabolic Regulation Mechanism Analysis", who diseased on 20 April, 2010. We acknowledge him for his continuous encouragement and support.

This work was supported in part by a CREST grant (to Y. F. and Y. S.) from the Science and Technology Agency of Japan; Grant-in-Aid for Scientific Research on Priority Areas 18076002 (Y.S.) and 19058011 (Y.F.), Grants-in-Aid for Scientific Research (B) 22380052 (Y.S.) and (B) 20370039 (Y.F.), Cooperative Grant of National Project on Protein Structural and Functional Analyses (to Y.F.), and The 21st Century COE and Global COE Programs from the Ministry of Education, Culture, Sports, Science and Technology of Japan, grant from Japan Foundation for Applied Enzymology (to Y.F.). A.I. is a CREST Research Assistant Fellow.

REFERENCES

1. **Azevedo, D., F. Tacnet, A. Delaunay, C. Rodrigues-Pousada, and M. B. Toledano.** 2003. Two redox centers within Yap1 to H_2O_2 and thiol-reactive chemicals signaling. Free Radic. Biol. Med. **35:**889-900.

2. **Baumgart, E., I. Vanhorebeek, M. Grabenbauer, M. Borgers, P. E. Declercq, H. D. Fahimi, and M. Baes.** 2001. Mitochondrial alterations caused by defective peroxisomal biogenesis in a mouse model for Zellweger syndrome (*PEX5* knockout mouse). Am. J. Pathol. **159:**1477-1494.

3. **Belousov, V. V., A. F. Fradkov, K. A. Lukyanov, D. B. Staroverov, K. S. Shakhbazov, A. V. Terskikh, and S. Lukyanov.** 2006. Genetically encoded fluorescent indicator for intracellular hydrogen peroxide. Nat. Methods **3:**281-286.

4. **Dooley, C. T., T. M. Dore, G. T. Hanson, W. C. Jackson, S. J. Remington, and R. Y. Tsien.** 2004. Imaging dynamic redox changes in mammalian cells with green fluorescent protein indicators. J. Biol. Chem. **279:**22284-22293.

5. **Fujiki, Y., K. Okumoto, N. Kinoshita, and K. Ghaedi.** 2006. Lessons from peroxisome-deficient Chinese hamster ovary (CHO) cell mutants. Biochim. Biophys. Acta **1763:**1374-81.

6. **Griesbeck, O., G. Baird, R. E. Campbell, D. A. Zacharias, and R. Y. Tsien.** 2001. Reducing the environmental sensitivity of yellow fluorescent protein. J. Biol. Chem. **276:**29188-29194.

7. **Hanson, G. T., R. Aggeler, D. Oglesbee, M. Cannon, R. A. Capaldi, R. Y. Tsien, and S. J. Remington.** 2004. Investigating mitochondrial redox potential with redox-sensitive green fluorescent protein indicators. J. Biol. Chem. **279:**13044-13053.

8. **Hayes, J. D., and D. J. Pulford.** 1995. The glutathione S-transferase supergene family: regulation of GST and the contribution of the isozymes to cancer chemoprotection and drug resistance. Crit. Rev. Biochem. Mol. Biol. **30:**445-600.

9. **Horiguchi, H., H. Yurimoto, N. Kato, and Y. Sakai.** 2001. Antioxidant system within yeast peroxisome: biochemical and physiological characterization of CbPmp20 in the methylotrophic yeast *Candida boidinii*. J. Biol. Chem. **276:**14279-14288.

10. **Hwang, C., A. J. Sinskey, and H. F. Lodish.** 1992. Oxidized redox state of glutathione in the endoplasmic reticulum. Science **257:**1496-1502.

11. **Kasischke, K. A., H. D. Vishwasrao, P. J. Fischer, W. R. Zipfel, and W. W. Webb.** 2004. Neural activity triggers neuronal oxidative metabolism followed by astrocytic glycolysis. Science **305:**99-103.

12. **Kawada, Y., M. Khan, A. K. Sharma, D. B. Ratnayake, K. Dobashi, K. Asayama, H. W. Moser, M. A. Contreras, and I. Singh.** 2004. Inhibition of peroxisomal functions due to oxidative imbalance induced by mistargeting of catalase to cytoplasm is restored by vitamin E treatment in skin fibroblasts from Zellweger syndrome-like patients. Mol. Genet. Metab. **83:**297-305.

13. **Kemp, M., Y. M. Go, and D. P. Jones.** 2008. Nonequilibrium thermodynamics of thiol/disulfide redox systems: a perspective on redox systems biology. Free Radic. Biol. Med. **44:**921-937.

14. **Kosower, N. S., and E. M. Kosower.** 1978. The glutathione status of cells. *Int. Rev. Cytol*. **54:**109-160.

15. **Kozak, M.** 1989. The scanning model for translation: an update. J. Cell Biol **108:**229-241.

16. **Kuge, S., N. Jones, N. Iizuka, and A. Nomoto.** 1998. Crm1 (XpoI)-dependent nuclear export of the budding yeast transcription factor yAP-1 is sensitive to oxidative stress. Genes Cells **3:**521-532.

17. **Lohman, J. R., and S. J. Remington.** 2008. Development of a family of redox-sensitive green fluorescent protein indicators for use in relatively oxidizing subcellular environments. Biochemistry **47:**8678-8688.

18. **McGuinness, M. C., J. F. Lu, H. P. Zhang, G. X. Dong, A. K. Heinzer, P. A. Watkins, J. Powers, and K. D. Smith.** 2003. Role of ALDP (ABCD1) and mitochondria in X-linked adrenoleukodystrophy. Mol. Cell. Biol. **23:**744-753.

19. **McGuinness, M. C., H. Wei, and K. D. Smith.** 2000. Therapeutic developments in peroxisome biogenesis disorders. Expert Opin. Investig. Drugs **9:**1985-1992.

20. **McGuinness, M. C., H. P. Zhang, and K. D. Smith.** 2001. Evaluation of pharmacological induction of fatty acid β-oxidation in X-linked adrenoleukodystrophy. Mol. Genet. Metab. **74:**256-263.

21. **Monosov, E. D., T. J. Wenzel, G. H. Lüers, J. A. Heyman, and S. Subramani.** 1996. Labeling of peroxisomes with green fluorescent protein in living *P. pastoris* cells. J. Histochem. Cytochem. **44:**581-589.

22. **Okazaki, S., A. Naganuma, and S. Kuge.** 2005. Peroxiredoxin-mediated redox regulation of the nuclear localization of Yap1, a transcription factor in budding yeast. Antioxid. Redox Signal. **7:**327-334.

23. **Østergaard, H., A. Henriksen, F. G. Hansen, and J. R. Winther.** 2001. Shedding light on disulphide bond formation: engineering a redox switch in green fluorescent protein. EMBO J. **20:**5853-5862.

24. **Østergaard, H., C. Tachibana, and J. R. Winther.** 2004. Monitoring disulphide bond formation in the eukaryotic cytosol. J. Cell Biol. **166:**337-345.

25. **Otera, H., T. Harano, M. Honsho, K. Ghaedi, S. Mukai, A. Tanaka, A. Kawai, N. Shimizu, and Y. Fujiki.** 2000. The mammalian peroxin Pex5pL, the longer isoform of the mobile peroxisome targeting signal (PTS) type 1 transporter, translocates the Pex7p·PTS2 protein complex into peroxisomes via its initial docking site, Pex14p. J. Biol. Chem. **275:**21703-21704.

26. **Poirier, Y., V. D. Antonenkov, T. Glumoff, and J. K. Hiltunen.** 2006. Peroxisomal beta-oxidation--a metabolic pathway with multiple functions. Biochim. Biophys. Acta **1763:**1413-26.

27. **Powis, G., J. R. Gasdaska, and A. Baker.** 1997. Redox signaling and the control of cell growth and death. Adv. Pharmacol. **38:**329-359.

28. **Rizzo, M. A., G. H. Springer, B. Granada, and D. W. Piston.** 2004. An improved cyan fluorescent protein variant useful for FRET. Nat. Biotechnol. **22:**445-449.

29. **Rost, J., and S. Rapoport.** 1964. Reduction-potential of glutathione. Nature **201:**185.

30. **Sakai, Y., A. Koller, L. K. Rangell, G. A. Keller, and S. Subramani.** 1998. Peroxisome degradation by micropexophagy in *Pichia pastoris*: identification of specific steps and morphological intermediates. J. Cell Biol. **141:**625-636.

31. **Schrader, M., and H. D. Fahimi.** 2006. Peroxisomes and oxidative stress. Biochim. Biophys. Acta **1763:**1755-1766.

32. **Sears, I. B., J. O'Connor, O. W. Rossanese, and B. S. Glick.** 1998. A versatile set of vectors for constitutive and regulated gene expression in *Pichia pastoris*. Yeast **14:**783-790.

33. **Steinberg, S. J., G. Dodt, G. V. Raymond, N. E. Braverman, A. B. Moser, and H. W. Moser.** 2006. Peroxisome biogenesis disorders. Biochim. Biophys. Acta **1763:**1733-1748.

34. **T. Jubany-Mari, L. A.-B., K. Jiang, L.J. Feldman.** 2010. Use of a redox-sensing GFP (c-roGFP1) for real-time monitoring of cytosol redox status in Arabidopsis thaliana water-stressed plants. FEBS Letters, *in press*.

35. **Tietze, F.** 1969. Enzymatic method for quantitative determination of nanogram amounts of total and oxidized glutathione: applications to mammalian blood and other tissues. Anal. Biochem. **27:**502-506.

36. **Tsukamoto, T., S. Yokota, and Y. Fujiki.** 1990. Isolation and characterization of Chinese hamster ovary cell mutants defective in assembly of peroxisomes. J. Cell Biol. **110:**651-660.

37. **van der Klei, I. J., and M. Veenhuis.** 2006. Yeast and filamentous fungi as model organisms in microbody research. Biochim. Biophys. Acta **1763:**1364-73.

38. **Wei, H., S. Kemp, M. C. McGuinness, A. B. Moser, and K. D. Smith.** 2000. Pharmacological induction of peroxisomes in peroxisome biogenesis disorders. Ann. Neurol. **47:**281-283.

39. **Yurimoto, H., B. Lee, T. Yano, Y. Sakai, and N. Kato.** 2003. Physiological role of S-formylglutathione hydrolase in C(1) metabolism of the methylotrophic yeast Candida boidinii. Microbiology **149:**1971-9.

40. **Zhang, Q., D. W. Piston, and R. H. Goodman.** 2002. Regulation of corepressor function by nuclear NADH. Science **295:**1895-1897.

Figure legends

FIG. 1. The domain structure, schematic representation and *in vitro* characterization of Redoxfluor. (A) Schematic drawing of Yap1 comprising a basic leucine-zipper DNA-binding domain (bZIP), an n-CRD (N279 to R313), and a c-CRD (N565 to N650). Redoxfluor comprises a fusion of Cerulean, a tandemly repeated fragment of the Yap1 c-CRD (I601 to N650), and Citrine. (B) Emission spectra of Redoxfluor before (black) and after (red) exposure to H_2O_2 (100 μM) at 434 nm excitation. (C) Responses of Redoxfluor C-probe (red) and A-probe (black) to various reagents. The purified probes were incubated with H_2O_2 (100 μM), ATZ (10 mM), or BSO (100 μM) until the emission intensities following 434 nm excitation reached constant values. The FRET ratios (YFP intensity /CFP intensity) are shown relative to those obtained from untreated control samples. The data represent the means ± s.d. (n=3).

FIG. 2. Redox titration of Redoxfluor with reduced and oxidized glutathione *in vitro*. (A) Spectrophotometric analysis of C-probe (red) and A-probe (blue) at 37°C in titration buffer containing different ratios of GSH/GSSG corresponding to the designated electropotential (E_0') gradient. The excitation wavelength was 405 nm (open circles) or 434 nm (closed circles). (B) mPEG-maleimide modification of Redoxfluor. Under the same titration conditions as in (A), the purified Redoxfluor was incubated with mPEG-maleimide and subjected to immunoblot analysis. The arrows indicate the signals corresponding to the non-modified form of the protein. The asterisks indicate signals corresponding to modified forms of the probe protein.

FIG. 3. Visualization of the redox state in yeast and CHO-K1 cells. (A) Imaging of the FRET signal generated by wild-type (C-probe) or mutant (A-probe) Redoxfluor in *S. cerevisiae* in response to H_2O_2 (100 μM), ATZ (10 mM), or BSO (100 μM). Following exposure of cells to H_2O_2 or ATZ, the cells were incubated in fresh (drug-free) medium, and were monitored at the indicated times. Bar, 2 μm. (B) The FRET ratio imaging of C-probe in CHO-K1 cells in response to H_2O_2 (100 μM) or ATZ (10 mM) (Video 1 and Video 2). ATZ-treatment of CHO-K1 cells expressing A-probe did not show a C-probe like FRET response, although a slight FRET change due to the inherent redox-responsive nature of the fluorescent protein was observed. Bar, 10 μm. (C) From the microscopic analyses shown in (B), the relative values of the FRET signal intensity of the C-probe before and after H_2O_2 or ATZ treatment were plotted.

FIG. 4. Targeting of Redoxfluor to peroxisomes in mammalian and yeast cells. (A) The intraperoxisomal redox state assessed by C-probe-PTS1 is more reductive than the cytosolic redox state in ~~a~~ wild-type CHO cells. The FRET-ratio images of A-probe-PTS1 (lacking the redox-sensitive cysteine residues) and of cytosolic C-probe are also shown as controls. Bar, 10 μm. The FRET values of the Redoxfluor probes are normalized to the value generated with the cytosolic C-probe which was arbitrarily set to 1.0. (B) The intraperoxisomal C-probe is functional (CHO cells). The intraperoxisomal redox change represented by FRET ratio imaging of C-probe-PTS1 (also see Video 3). (C) A *P. pastoris* wild-type strain PPY12 expressing C-probe-PTS1 was transferred to oleate or methanol medium for induction of peroxisome proliferation, and subjected to fluorescence microscopy for the FRET ratio imaging. Bar, 2 μm.

FIG. 5. The cytosolic redox state is reductive in CHO cells defective in peroxisome assembly. (A) Time course of the dynamics of the cytosolic redox state and peroxisome assembly in CHO-K1 and ZP105 cells. After incubation at 37°C, cells were cultured at 37°C or 30°C for 7 days. Bar, 10 μm. The import of GFP-PTS1, but not catalase, is restored in the ZP105 cell line after 7 days at 30°C, as shown in the lower panels. (B) Plotting of the relative values of the C-probe FRET signal intensity under the same culture condition as (A). (C) Relative abundance of *GST* mRNA, normalized to the levels of β-cytoskeletal actin (*ACTB*). (D) Intracellular glutathione redox ratio (GSH/GSSG).

FIG. 6. Redox states of *P. pastoris pex* mutant strains. (A) The cytosolic redox state is more reductive in the denoted *P. pastoris pex* mutants than in the wild-type (WT) strain during culture on oleate medium. Bar, 1 μm. The relative FRET values are normalized to the value generated from the probe in the wild-type strain, which was arbitrarily set to 1.0. (B) Transcription levels of antioxidant genes *PpGPX1*, *PpTSA1*, *PpCTA1*, and *PpSOD2*, in wild-type and *Pppex5*Δ strains. Values represent the means ± s.d. (n=3).

FIG. 7. Redox modulators, pharmacological agents that restore the intracellular redox state of mutant cell lines to normal levels. (A) FRET imaging of CHO cells at 37°C treated with TSA (50 nM), VE (50 M), and 4PBA (5 mM). Bar, 10 μm. (B) The values represent the relative FRET values of Redoxfluor normalized to the value from non-treated CHO-K1 (wild-type) set arbitrarily to 1.0. (C) The relative abundance of *GST* mRNA standardized against the levels for *ACTB*. (D) Intracellular GSH/GSSG ratio. In (B) and (C), values represent the means ± s.d. (n=3).

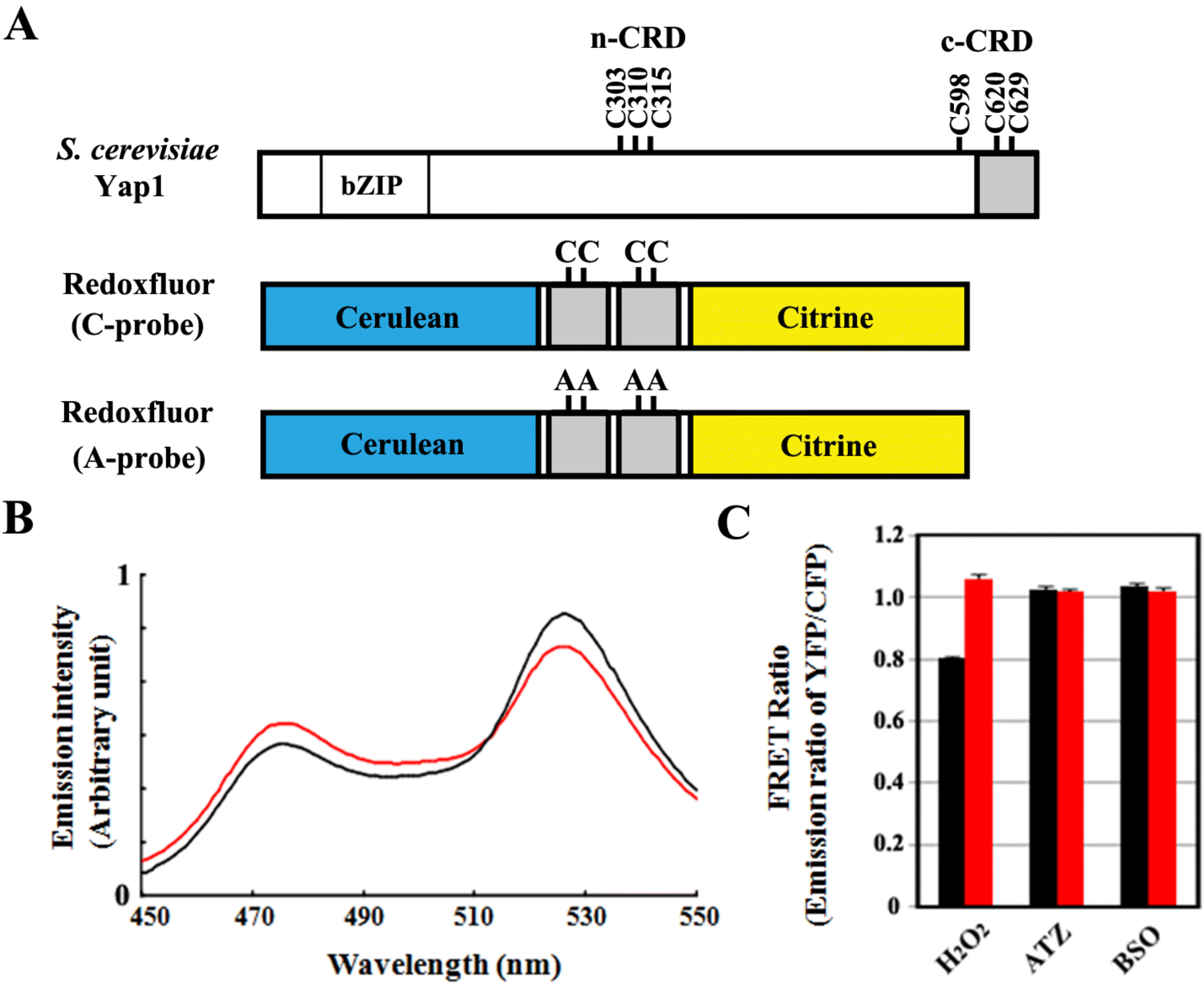

Figure 1 Yano et al

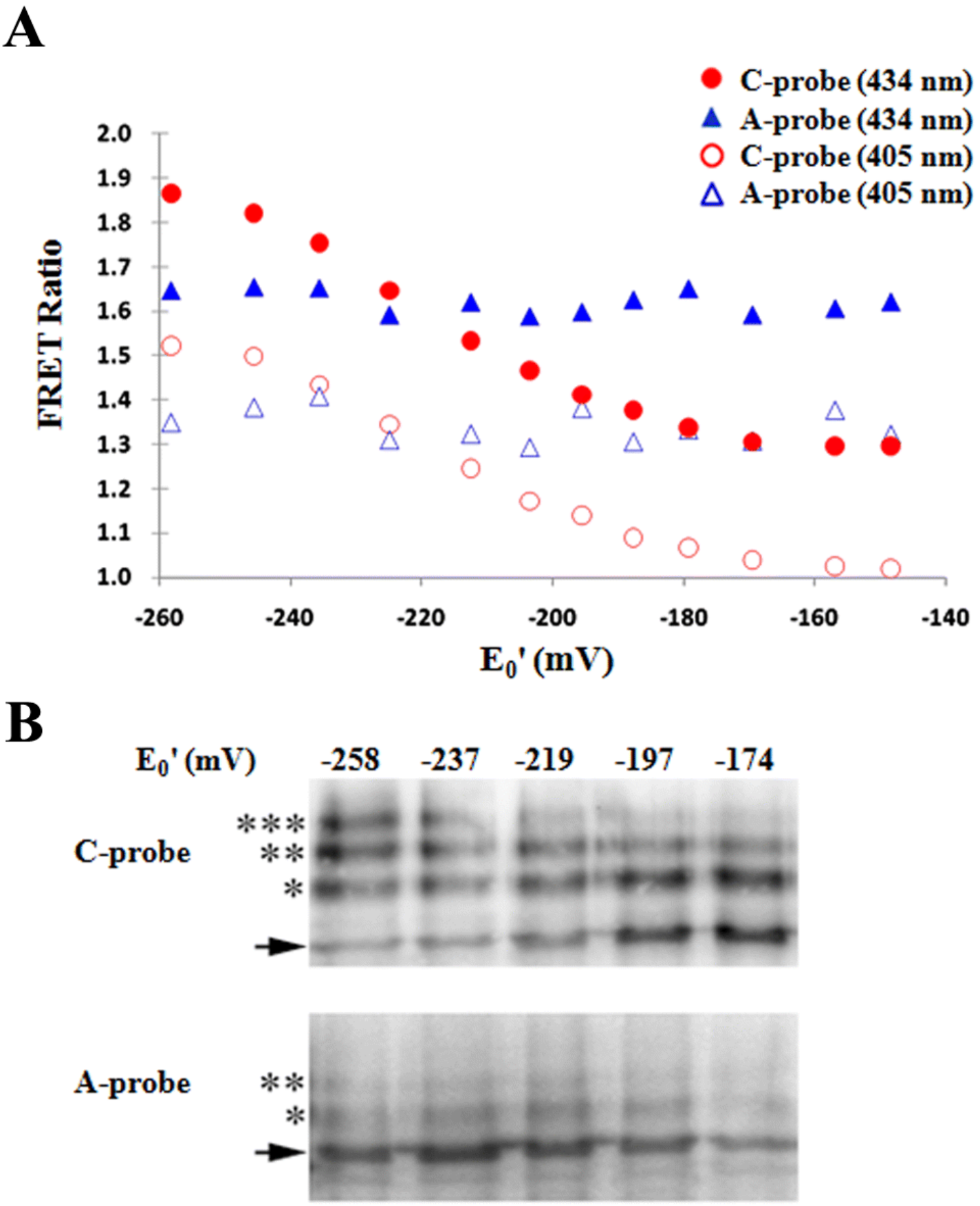

Figure 2 Yano et al

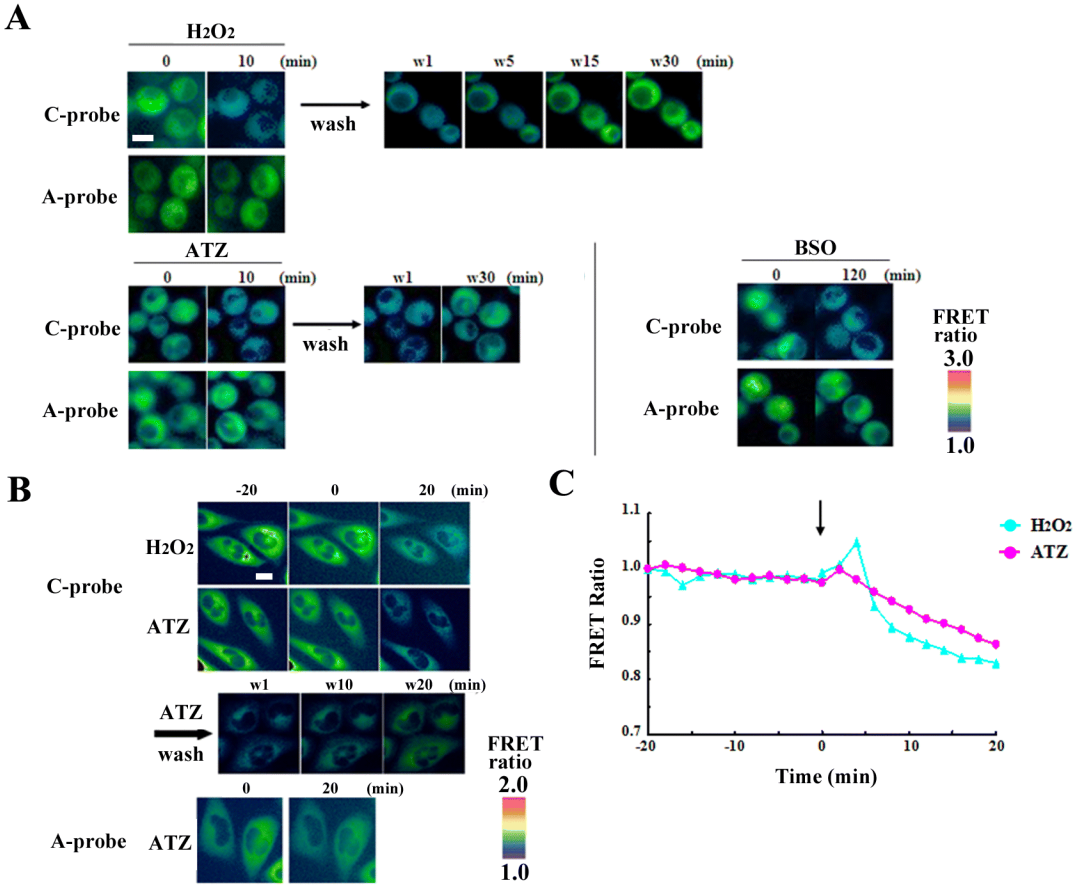

Figure 3 Yano et al

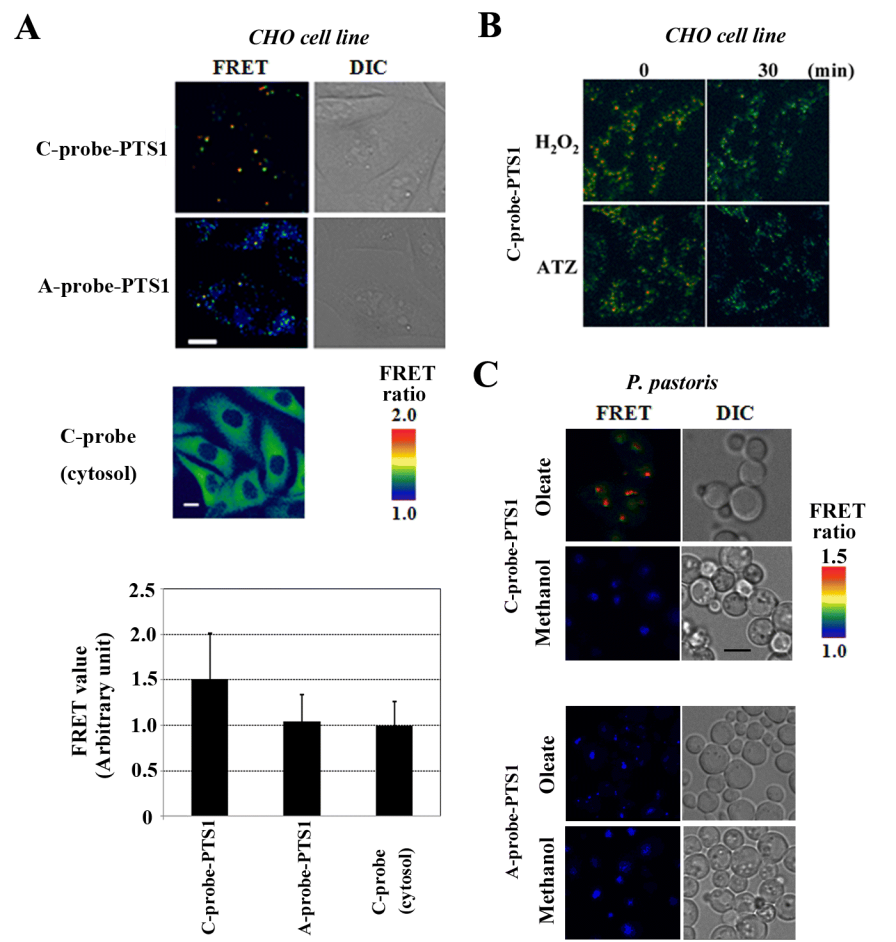

Figure 4 Yano et al

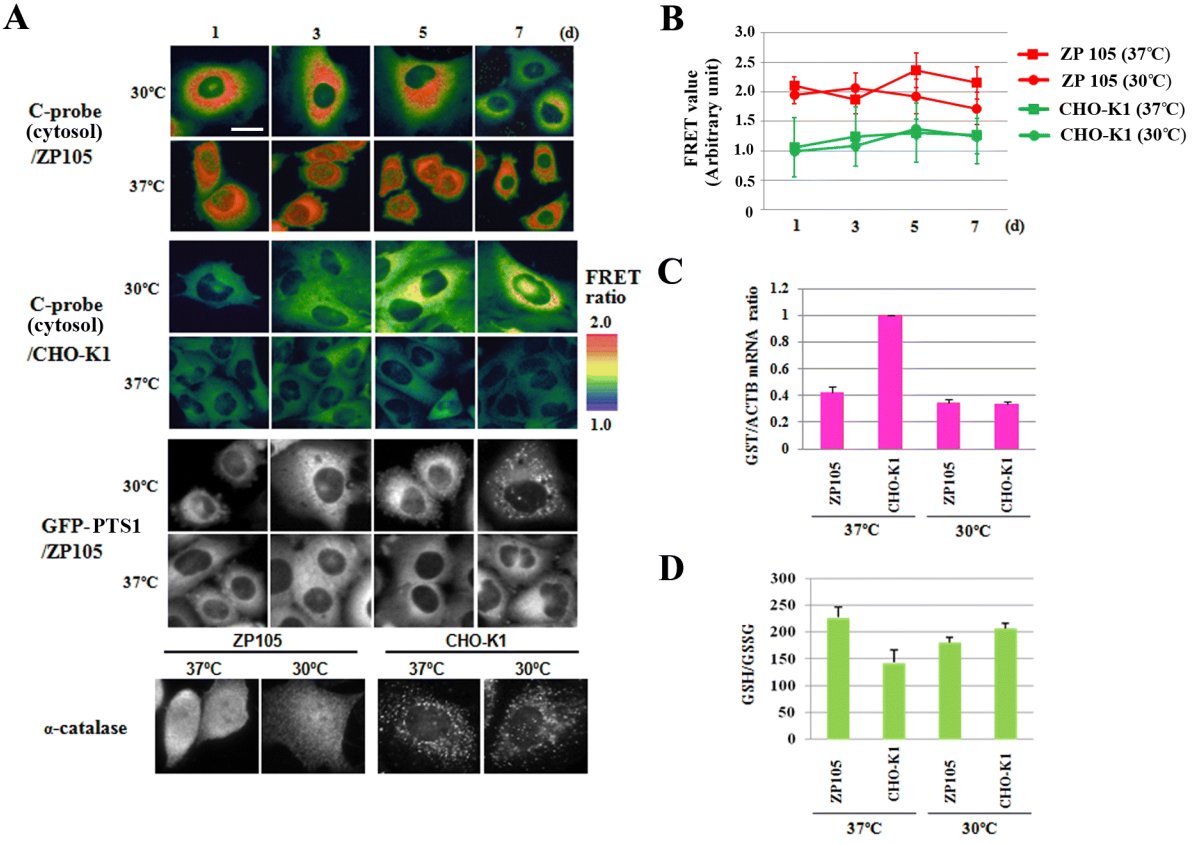

Figure 5 Yano et al

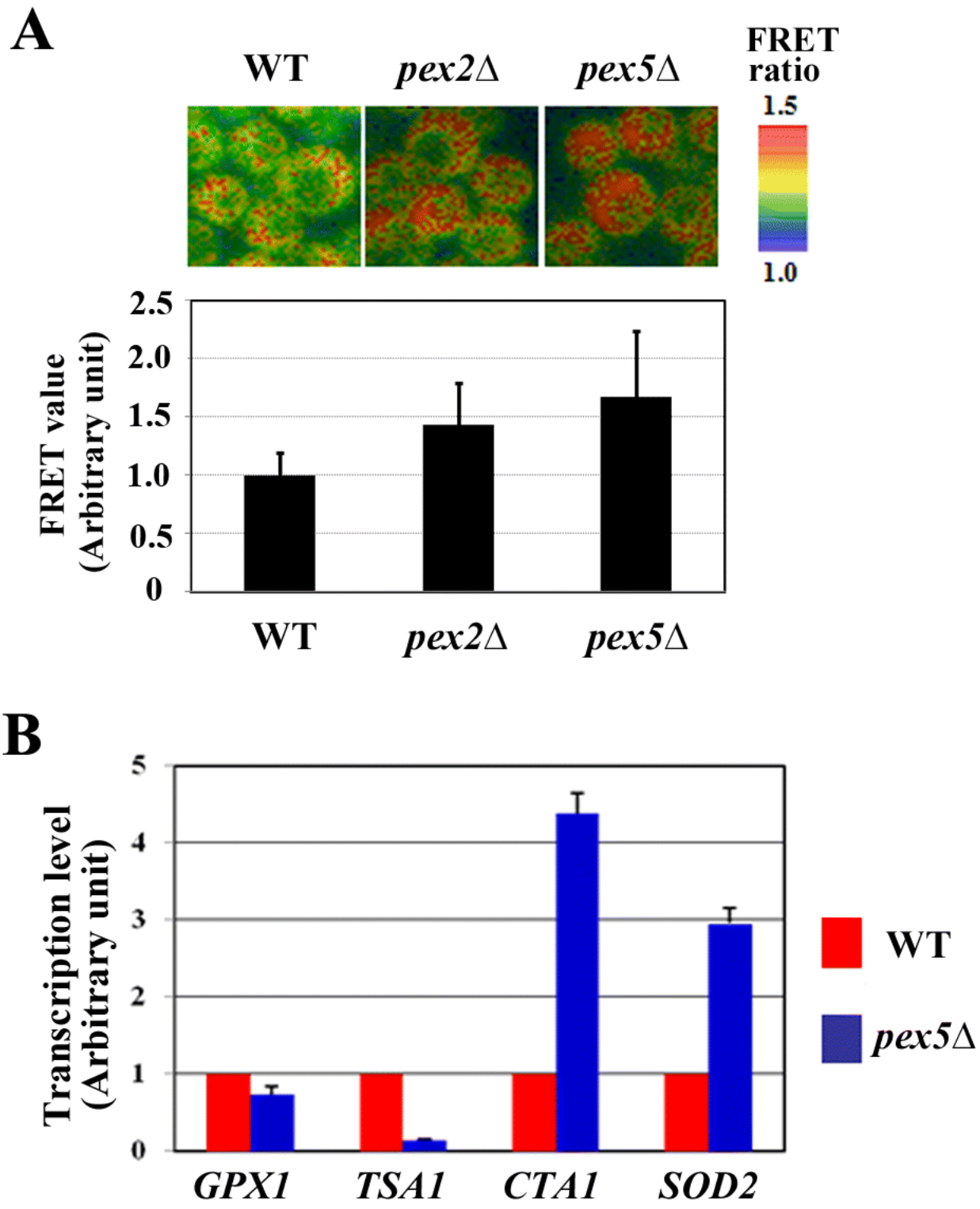

Figure 6 Yano et al

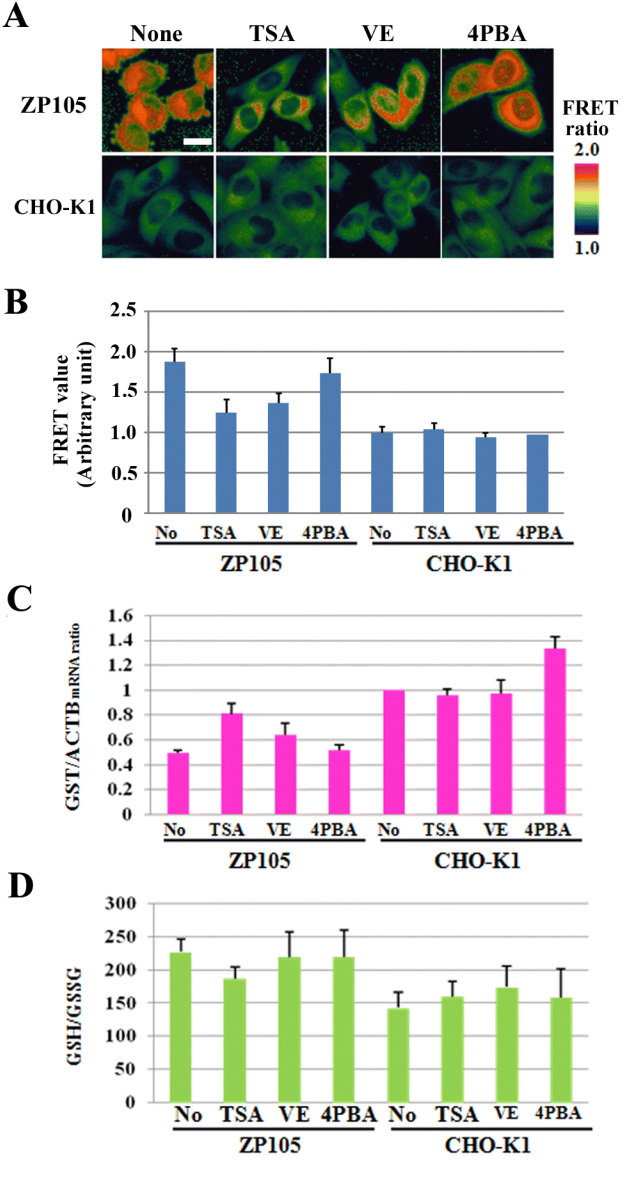

Figure 7 Yano et al